

Fast MCMC Sampling for Markov Jump Processes and Extensions

Vinayak Rao*

*Department of Statistical Science
Duke University
Durham, NC, 27708-0251, USA*

VRAO@GATSBY.UCL.AC.UK

Yee Whye Teh

*Department of Statistics
1 South Parks Road
Oxford OX1 3TG, UK*

Y.W.TEH@STATS.OX.AC.UK

Accepted for publication in the Journal of Machine Learning Research (JMLR)

Editor: Christopher Meek

Abstract

Markov jump processes (or continuous-time Markov chains) are a simple and important class of continuous-time dynamical systems. In this paper, we tackle the problem of simulating from the posterior distribution over paths in these models, given partial and noisy observations. Our approach is an auxiliary variable Gibbs sampler, and is based on the idea of *uniformization*. This sets up a Markov chain over paths by alternately sampling a finite set of virtual jump times given the current path, and then sampling a new path given the set of extant and virtual jump times. The first step involves simulating a piecewise-constant inhomogeneous Poisson process, while for the second, we use a standard hidden Markov model forward filtering-backward sampling algorithm. Our method is exact and does not involve approximations like time-discretization. We demonstrate how our sampler extends naturally to MJM-based models like Markov-modulated Poisson processes and continuous-time Bayesian networks, and show significant computational benefits over state-of-the-art MCMC samplers for these models.

Keywords: Markov jump process, MCMC, Gibbs sampler, uniformization, Markov-modulated Poisson process, continuous-time Bayesian network

1. Introduction

The Markov jump process (MJP) extends the discrete-time Markov chain to continuous time, and forms a simple and popular class of continuous-time dynamical systems. In Bayesian modelling applications, the MJP is widely used as a prior distribution over the piecewise-constant evolution of the state of a system. The Markov property of the MJP makes it both a realistic model for various physical and chemical systems, as well as a convenient approximation for more complex phenomena in biology, finance, queuing systems etc. In chemistry and biology, stochastic kinetic models use the state of an MJP to represent the sizes of various interacting *species* (e.g., Gillespie, 1977; Golightly and Wilkinson, 2011). In queuing applications, the state may represent the number of pending jobs in a queue (Breuer, 2003; Tijms, 1986), with the arrival and processing of jobs treated as memoryless events. MJPs find wide application in genetics, for example, an MJP trajectory is sometimes used

*. Corresponding author

to represent a segmentation of a strand of genetic matter. Here ‘time’ represents position along the strand, with particular motifs occurring with different rates in different regions (Fearnhead and Sherlock, 2006). MJPs are also widely used in finance, for example, Elliott and Osakwe (2006) use an MJP to model switches in the parameters that govern the dynamics of stock prices (the latter being modelled with a Lévy process).

In the Bayesian setting, the challenge is to characterize the posterior distribution over MJP trajectories given noisy observations; this typically cannot be performed analytically. Various sampling-based (Fearnhead and Sherlock, 2006; Boys et al., 2008; El-Hay et al., 2008; Fan and Shelton, 2008; Hobolth and Stone, 2009) and deterministic (Nodelman et al., 2002, 2005; Opper and Sanguinetti, 2007; Cohn et al., 2010) approximations have been proposed in the literature, but come with problems: they are often generic methods that do not exploit the structure of the MJP, and when they do, involve expensive computations like matrix exponentiation, matrix diagonalization or root-finding, or are biased, involving some form of time-discretization or independence assumptions. Moreover, these methods do not extend easily to more complicated likelihood functions which require specialized algorithms (for instance, the contribution of Fearnhead and Sherlock (2006) is to develop an exact sampler for Markov-modulated Poisson processes (MMPPs), where an MJP modulates the rate of a Poisson process).

In this work, an extension of Rao and Teh (2011a), we describe a novel Markov chain Monte Carlo (MCMC) sampling algorithm for MJPs that avoids the need for the expensive computations described previously, and does not involve any form of approximation (i.e., our MCMC sampler converges to the true posterior). Importantly, our sampler is easily adapted to complicated extensions of MJPs such as MMPPs and continuous-time Bayesian networks (CTBNs) (Nodelman et al., 2002), and is significantly more efficient than the specialized samplers developed for these models. Like many existing methods, our sampler introduces auxiliary variables which simplify the structure of the MJP, using an idea called *uniformization*. Importantly, unlike some existing methods which produce *independent* posterior samples of these auxiliary variables, our method samples these *conditioned* on the current sample trajectory. While the former approach depends on the observation process, and can be hard for complicated likelihood functions, ours results in a simple distribution over the auxiliary variables that is independent of the observations. The observations are accounted for during a straightforward discrete-time forward-filtering backward-sampling step to resample a new trajectory. The overall structure of our algorithm is that of an auxiliary variable Gibbs sampler, alternately resampling the auxiliary variables given the MJP trajectory, and the trajectory given the auxiliary variables.

In Section 2 we briefly review Markov jump processes. In Section 3 we introduce the idea of uniformization and describe our MCMC sampler for the simple case of a discretely observed MJP. In Section 4, we apply our sampler to the Markov-modulated Poisson process, while in Section 5, we describe continuous-time Bayesian networks, and extend our algorithm to that setting. In both sections, we report experiments comparing our algorithm to state-of-the-art sampling algorithms developed for these models. We end with a discussion in Section 6.

2. Markov Jump Processes (MJPs)

A Markov jump process ($\mathbf{S}(t)$, $t \in \mathbb{R}_+$) is a stochastic process with right-continuous, piecewise-constant paths (see for example Çinlar, 1975). The paths themselves take values in some countable space $(\mathcal{S}, \Sigma_{\mathcal{S}})$, where $\Sigma_{\mathcal{S}}$ is the discrete σ -algebra. As in typical applications, we assume \mathcal{S} is finite

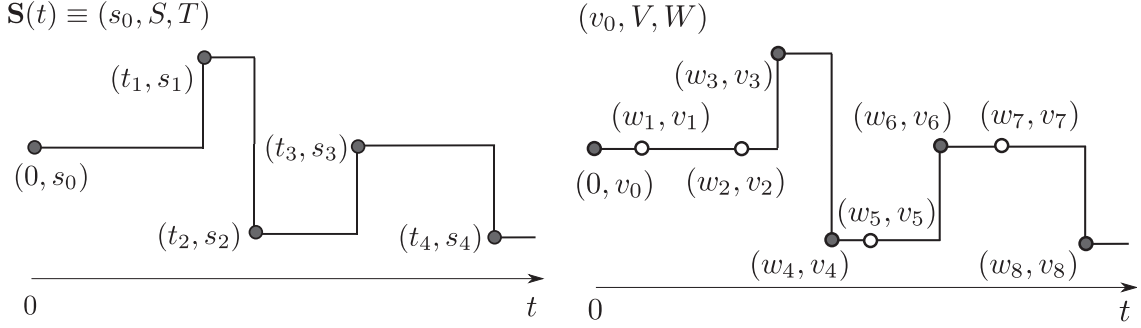


Figure 1: (left) An MJP path (s_0, S, T) , (right) a uniformized representation (v_0, V, W) .

(say $\mathcal{S} = \{1, 2, \dots, N\}$). We also assume the process is homogeneous, implying (together with the Markov property) that for all times $t, t' \in \mathbb{R}_+$ and states $s, s' \in \mathcal{S}$,

$$p(\mathbf{S}(t' + t) = s | \mathbf{S}(t') = s', (\mathbf{S}(u), u < t')) = [P_t]_{ss'}$$

for some stochastic matrix P_t that depends only on t . The family of transition matrices $(P_t, t \geq 0)$ is defined by a matrix $A \in \mathbb{R}^{N \times N}$ called the *rate matrix* or *generator* of the MJP. A is the time-derivative of P_t at $t = 0$, with

$$\begin{aligned} P_t &= \exp(At), \\ p(\mathbf{S}(t' + dt) = s | \mathbf{S}(t') = s') &= A_{ss'} dt \quad (\text{for } s \neq s'), \end{aligned} \tag{1}$$

where Equation (1) is the matrix exponential. The off-diagonal elements of A are nonnegative, and represent the rates of transiting from one state to another. Its diagonal entries are $A_s \equiv A_{ss} = -\sum_{s' \neq s} A_{s's}$ for each s , so that its columns sum to 0, with $-A_s = |A_s|$ characterizing the total rate of leaving state s .

Consider a time interval $\mathcal{T} \equiv [t_{start}, t_{end}]$, with the Borel σ -algebra $\Sigma_{\mathcal{T}}$. Let π_0 be a density with respect to the counting measure $\mu_{\mathcal{S}}$ on $(\mathcal{S}, \Sigma_{\mathcal{S}})$; this defines the initial distribution over states at t_{start} . Then an MJP is described by the following generative process over paths on this interval, commonly called *Gillespie's algorithm* (Gillespie, 1977):

Algorithm 1 Gillespie's algorithm to sample an MJP path on the interval $[t_{start}, t_{end}]$

Input: The rate matrix A and the initial distribution over states π_0 .
Output: An MJP trajectory $\mathbf{S}(t) \equiv (s_0, S, T)$.

- 1: Assign the MJP a state $s_0 \sim \pi_0$. Set $t_0 = t_{start}$ and $i = 0$.
 - 2: **loop**
 - 3: Draw $z \sim \exp(|A_{s_i}|)$.
 - 4: **If** $t_i + z > t_{end}$ **then return** $(s_0, \dots, s_i, t_1, \dots, t_i)$ **and stop**.
 - 5: Increment i and let $t_i = t_{i-1} + z$.
 - 6: The MJP jumps to a new state $s_i = s$ at time t_i , for an $s \neq s_{i-1}$,
 - 7: with probability proportional to $A_{ss_{i-1}}$.
 - 8: **end loop**
-

If all event rates are finite, an MJP trajectory will almost surely have only a finite number of jumps. Let there be n jumps, and let these occur at the ordered times (t_1, \dots, t_n) . Define $T \equiv (t_1, \dots, t_n)$, and let $S \equiv (s_1, \dots, s_n)$ be the corresponding sequence of states, where $s_i = \mathbf{S}(t_i)$. The triplet (s_0, S, T) completely characterizes the MJP trajectory over \mathcal{T} (Figure 1 (left)).

From Gillespie's algorithm, we see that sampling an MJP trajectory involves sequentially sampling $n + 1$ waiting times from exponential densities with one of N rates, and n new states from one of N discrete distributions, each depending on the previous state. The i th waiting time equals $(t_i - t_{i-1})$ and is drawn from an exponential with rate $|A_{s_{i-1}}|$, while the probability the i th state equals s_i is $A_{s_i s_{i-1}} / |A_{s_{i-1}}|$. The last waiting time can take any value greater than $t_{end} - t_n$. Thus, under an MJP, a random element (s_0, S, T) has density

$$\begin{aligned} p(s_0, S, T) &= \pi_0(s_0) \left(\prod_{i=1}^n |A_{s_{i-1}}| e^{-|A_{s_{i-1}}|(t_i - t_{i-1})} \frac{A_{s_i s_{i-1}}}{|A_{s_{i-1}}|} \right) \cdot e^{-|A_{s_n}|(t_{end} - t_n)} \\ &= \pi_0(s_0) \left(\prod_{i=1}^n A_{s_i s_{i-1}} \right) \exp \left(- \int_{t_{start}}^{t_{end}} |A_{\mathbf{S}(t)}| dt \right). \end{aligned} \quad (2)$$

To be precise, we must state the base measure with respect to which the density above is defined. The reader might wish to skip these details (and for more details, we recommend Daley and Vere-Jones, 2008). Let $\mu_{\mathcal{T}}$ be Lebesgue measure on \mathcal{T} . Recalling that the state space of the MJP is \mathcal{S} , we can view (S, T) as a sequence of elements in the product space $\mathcal{M} \equiv \mathcal{S} \times \mathcal{T}$. Let $\Sigma_{\mathcal{M}}$ and $\mu_{\mathcal{M}} = \mu_{\mathcal{S}} \times \mu_{\mathcal{T}}$ be the corresponding product σ -algebra and product measure. Define \mathcal{M}^n as the n -fold product space with the usual product σ -algebra $\Sigma_{\mathcal{M}}^n$ and product measure $\mu_{\mathcal{M}}^n$. Now let $\mathcal{M}^{\cup} \equiv \bigcup_{i=0}^{\infty} \mathcal{M}^i$ be a union space, elements of which represent finite length pure-jump paths¹. Let $\Sigma_{\mathcal{M}^{\cup}}$ be the corresponding union σ -algebra, where each measurable set $B \in \Sigma_{\mathcal{M}^{\cup}}$ can be expressed as $B = \bigcup_{i=0}^{\infty} B^i$ with $B^i = B \cap \mathcal{M}^i \in \Sigma_{\mathcal{M}}^i$. Assign this space the measure $\mu_{\mathcal{M}^{\cup}}$ defined as:

$$\mu_{\mathcal{M}^{\cup}}(B) = \sum_{i=0}^{\infty} \mu_{\mathcal{M}}^i(B^i).$$

Then, any element $(s_0, S, T) \in \mathcal{S} \times \mathcal{M}^{\cup}$ sampled from Gillespie's algorithm has density w.r.t. $\mu_{\mathcal{S}} \times \mu_{\mathcal{M}^{\cup}}$ given by Equation (2).

3. MCMC Inference via Uniformization

In this paper, we are concerned with the problem of sampling MJP paths over the interval $\mathcal{T} \equiv [t_{start}, t_{end}]$ given noisy observations of the state of the MJP. In the simplest case, we observe the process at the boundaries t_{start} and t_{end} . More generally, we are given the initial distribution over states π_0 as well as a set of O noisy observations $X = \{X_{t_1^o}, \dots, X_{t_O^o}\}$ at times $T^o = \{t_1^o, \dots, t_O^o\}$ with likelihoods $p(X_{t_i^o} | \mathbf{S}(t_i^o))$, and we wish to sample from the posterior $p(s_0, S, T | X)$. Here we have implicitly assumed that the observation times T^o are fixed. Sometimes the observation times themselves can depend on the state of the MJP, resulting effectively in *continuous-time* observations. This is the case for the Markov-modulated Poisson process and CTBNs. As we will show later, our method handles these cases quite naturally as well.

1. Define \mathcal{M}^0 as a point satisfying $\mathcal{M}^0 \times \mathcal{M} = \mathcal{M} \times \mathcal{M}^0 = \mathcal{M}$ (Daley and Vere-Jones, 2008).

A simple approach to inference is to discretize time and work with the resulting approximation. The time-discretized MJP corresponds to the familiar discrete-time Markov chain, and its Markov structure can be exploited to construct dynamic programming algorithms like the forward-filtering backward-sampling (FFBS) algorithm (Früwirth-Schnatter (1994); Carter and Kohn (1996); see also Appendix A) to sample posterior trajectories efficiently. However, time-discretization introduces a bias into our inferences, as the system can change state only at a fixed set of times, and as the maximum number of state changes is limited to a finite number. To control this bias, one needs to discretize time at a fine granularity, resulting in long Markov chains, and expensive computations.

Recently, there has been growing interest in constructing *exact* MCMC samplers for MJPs without any approximations such as time-discretization. We review these in Section 3.3. One class of methods exploits the fact an MJP can be exactly represented by a discrete-time Markov chain on a *random* time-discretization. Unlike discretization on a regular grid, a random grid can be quite coarse without introducing any bias. Given this discretization, we can use the FFBS algorithm to perform efficient sampling. However, we do not observe the random discretization, and thus also need to sample this from its posterior distribution. This posterior now depends on the likelihood process, and a number of algorithms attempt to solve this problem for specific observation processes. Our approach is to resample the discretization conditioned on the system trajectory. As we will see this is *independent* of the likelihood process, resulting in a simple, flexible and efficient MCMC sampler.

3.1 Uniformization

We first introduce the idea of *uniformization* (Jensen, 1953; Çinlar, 1975; Hobolth and Stone, 2009), which forms the basis of our sampling algorithm. For an MJP with rate-matrix A , choose some $\Omega \geq \max_s |A_s|$. Let $W = (w_1, \dots, w_{|W|})$ be an ordered set of times on the interval $[t_{start}, t_{end}]$ drawn from a homogeneous Poisson process with intensity Ω . W constitutes a random discretization of the time-interval $[t_{start}, t_{end}]$.

Next, letting I be the identity matrix, observe that $B = (I + \frac{1}{\Omega}A)$ is a stochastic matrix (it has nonnegative elements, and its columns sum to one). Run a discrete-time Markov chain with initial distribution π_0 and transition matrix B on the times in W ; this is a Markov chain *subordinated* to the Poisson process W . The Markov chain will assign a set of states (v_0, V) ; v_0 at the initial time t_{start} , and $V = (v_1, \dots, v_{|V|})$ at the discretization times W (so that $|V| = |W|$). In particular, v_0 is drawn from π_0 , while v_i is drawn from the probability vector given by the v_{i-1} th column of B . Just as (s_0, S, T) characterizes an MJP path, (v_0, V, W) also characterizes a sample path of some piecewise-constant, right-continuous stochastic process on $[t_{start}, t_{end}]$. Observe that the matrix B allows self-transitions, so that unlike S , V can jump from a state back to the same state. We treat these as *virtual* jumps, and regard (v_0, V, W) as a redundant representation of a pure-jump process that always jumps to a new state (see Figure 1 (right)). The virtual jumps provide a mechanism to ‘thin’ the set W , thereby rejecting some of its events. This corrects for the fact that since the Poisson rate Ω dominates the leaving rates of all states of the MJP, W will on average contain more events than there are jumps in the MJP path. As the parameter Ω increases, the number of events in W increases; at the same time the diagonal entries of B start to dominate, so that the number of self-transitions (thinned events) also increases. The next proposition shows that these two effects exactly compensate each other, so that the process characterized by (v_0, V, W) is precisely the desired MJP.

Proposition 1 (*Jensen, 1953*) For any $\Omega \geq \max_s |A_s|$, (s_0, S, T) and (v_0, V, W) define the same Markov jump process $\mathbf{S}(t)$.

Proof We follow Hobolth and Stone (2009). From Equation (1), the marginal distribution of the MJP at time t is given by

$$\begin{aligned} \pi_t &= \exp(At)\pi_0 \\ &= \exp(\Omega(B-I)t)\pi_0 \\ &= \exp(-\Omega t)\exp(\Omega t B)\pi_0 \\ &= \sum_{n=0}^{\infty} \left(\left(\exp(-\Omega t) \frac{(\Omega t)^n}{n!} \right) (B^n \pi_0) \right). \end{aligned}$$

The first term in the summation is the probability that a rate Ω Poisson produces n events in an interval of length t , i.e., that $|W| = n$. The second term gives the marginal distribution over states for a discrete-time Markov chain after n steps, given that the initial state is drawn from π_0 , and subsequent states are assigned according to a transition matrix B . Summing over n , we obtain the marginal distribution over states at time t . Since the transition kernels induced by the uniformization procedure agree with those of the Markov jump process ($\exp(At)$) for all t , and since the two processes also share the same initial distribution of states, π_0 , all finite dimensional distributions agree. Following Kolmogorov's extension theorem (Kallenberg, 2002), both define versions of the same stochastic process. ■

A more direct but cumbersome approach is note that (v_0, V, W) is also an element of the space $\mathcal{S} \times \mathcal{M}^\cup$. We can then write down its density $p(v_0, V, W)$ w.r.t. $\mu_S \times \mu^\cup$, and show that marginalizing out the number and locations of self-transitions recovers Equation (2). While we do not do this, we will derive the density $p(v_0, V, W)$ for later use. As in Section 2, let \mathcal{T}^\cup and \mathcal{S}^\cup denote the measure spaces consisting of finite sequences of times and states respectively, and let $\mu_{\mathcal{T}}^\cup$ and $\mu_{\mathcal{S}}^\cup$ be the corresponding base measures. The Poisson realization W is determined by waiting times sampled from a rate Ω exponential distribution, so that following Equation (2), W has density w.r.t. $\mu_{\mathcal{T}}^\cup$ given by

$$p(W) = \Omega^{|W|} e^{-\Omega(t_{end} - t_{start})}. \quad (3)$$

Similarly, from the construction of the Markov chain, it follows that the state assignment (v_0, V) has probability density w.r.t. $\mu_S \times \mu_{\mathcal{S}}^\cup$ given by

$$p(v_0, V|W) = \pi_0(v_0) \prod_{i=1}^{|V|} \left(1 + \frac{A_{v_i}}{\Omega} \right)^{1(v_i=v_{i-1})} \left(\frac{A_{v_i v_{i-1}}}{\Omega} \right)^{1(v_i \neq v_{i-1})}.$$

Since under uniformization $|V| = |W|$, it follows that

$$\begin{aligned} \mu_{\mathcal{S}}^\cup(dV) \times \mu_{\mathcal{T}}^\cup(dW) &= \mu_S^{|V|}(dV) \times \mu_{\mathcal{T}}^{|W|}(dW) \\ &= (\mu_{\mathcal{T}} \times \mu_S)^{|V|}(d(V, W)) \\ &= \mu_{\mathcal{M}}^\cup(d(V, W)). \end{aligned} \quad (4)$$

Thus, from Equations (3) and (4), (v_0, V, W) has density w.r.t. $\mu_S \times \mu_{\mathcal{M}}^{\cup}$ given by

$$p(v_0, V, W) = e^{-\Omega(t_{end}-t_{start})} \pi_0(v_0) \prod_{i=1}^{|V|} (\Omega + A_{v_i})^{1(v_i=v_{i-1})} (A_{v_i v_{i-1}})^{1(v_i \neq v_{i-1})}. \quad (5)$$

3.2 The MCMC Algorithm

We adapt the uniformization scheme described above to construct an auxiliary variable Gibbs sampler. Recall that the only difference between (s_0, S, T) and (v_0, V, W) is the presence of an auxiliary set of virtual jumps in the latter. Call the virtual jump times $U_{\mathcal{T}}$; associated with $U_{\mathcal{T}}$ is a sequence of states U_S . U_S is uniquely determined by (s_0, S, T) and $U_{\mathcal{T}}$ (see Figure 1(right)), and we say this configuration is *compatible*. Let $U = (U_S, U_{\mathcal{T}})$, and observe that for compatible values of U_S , (s_0, S, T, U) and (v_0, V, W) represent the same point in $\mathcal{S} \times \mathcal{M}^{\cup}$.

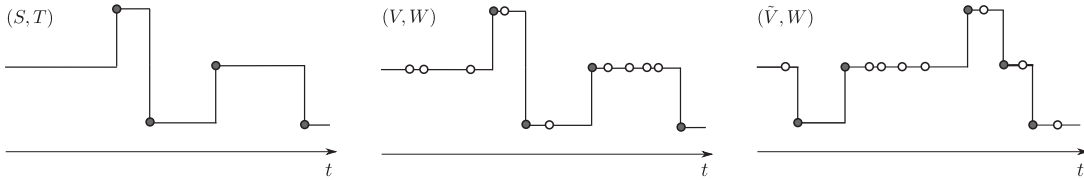


Figure 2: Uniformization-based Gibbs sampler: starting with an MJP trajectory (left), resample the thinned events (middle) and then resample the trajectory given all Poisson events (right). Discard the thinned events and repeat.

Given an MJP trajectory (s_0, S, T) (Figure 2 (left)), we proceed by first sampling the set of virtual jumps $U_{\mathcal{T}}$ given (s_0, S, T) , as a result recovering the uniformized characterization (s_0, V, W) (Figure 2 (middle)). This corresponds to a random discretization of $[t_{start}, t_{end}]$ at times W . We now discard the state sequence V , and perform a simple HMM forward-filtering backward-sampling step to resample a new state sequence \tilde{V} . Finally, dropping the virtual jumps in (s_0, \tilde{V}, W) gives a new MJP path $(s_0, \tilde{S}, \tilde{T})$. Figure 2 describes an iteration of the MCMC algorithm.

The next proposition shows that conditioned on (s_0, S, T) , the virtual jump times $U_{\mathcal{T}}$ are distributed as an *inhomogeneous* Poisson process with intensity $R(t) = \Omega + A_{S(t)}$ (we remind the reader that A has a negative diagonal, so that $R(t) \leq \Omega$). This intensity is piecewise-constant, taking the value $r_i = \Omega + A_{s_i}$ on the interval $[t_i, t_{i+1})$ (with $t_0 = t_{start}$ and $t_{n+1} = t_{end}$), so it is easy to sample $U_{\mathcal{T}}$ and thus U .

Proposition 2 *For any $\Omega \geq \max_s (|A_s|)$, both (s_0, S, T, U) and (v_0, V, W) have the same density w.r.t. $\mu_S \times \mu_{\mathcal{M}}^{\cup}$. In other words, the Markov jump process (s_0, S, T) along with virtual jumps U drawn from the inhomogeneous Poisson process as above is equivalent to the times W being drawn from a Poisson process with rate Ω , followed by the states (v_0, V) being drawn from the subordinated Markov chain.*

Proof Let $n = |T|$ be the number of jumps in the current MJP trajectory. Define $|U_i|$ as the number of auxiliary times in interval (t_i, t_{i+1}) . Then, $|U_{\mathcal{T}}| = \sum_{i=0}^n |U_i|$. If $U_{\mathcal{T}}$ is sampled from a piecewise-constant inhomogeneous Poisson process, its density is the product of the densities of a sequence of

homogeneous Poisson processes, and from Equation (3) is

$$p(U_{\mathcal{T}}|s_0, S, T) = \left(\prod_{i=0}^n (\Omega + A_{s_i})^{|U_i|} \right) \exp \left(- \int_{t_{start}}^{t_{end}} (\Omega + A_{S(t)}) dt \right) \quad (6)$$

w.r.t. $\mu_{\mathcal{T}}^{\cup}$. Having realized the times $U_{\mathcal{T}}$, the associated states U_S are determined too (elements of U_S in the interval (t_{i-1}, t_i) equal s_{i-1}). Thus $U = (U_S, U_{\mathcal{T}})$ given (s_0, S, T) has the same density as Equation (6), but now w.r.t. $\mu_{\mathcal{M}}^{\cup}$, and now restricted to elements of \mathcal{M}^{\cup} where U_S is compatible with $(S, T, U_{\mathcal{T}})$. Multiplying Equations (2) and (6), we see that (s_0, S, T, U) has density

$$p(s_0, S, T, U) = e^{-\Omega(t_{end}-t_{start})} \pi_0(s_0) \prod_{i=0}^n (\Omega + A_{s_i})^{|U_i|} \prod_{i=1}^n A_{s_i s_{i-1}}$$

w.r.t. $\mu_S \times \mu_{\mathcal{M}}^{\cup} \times \mu_{\mathcal{M}}^{\cup}$. However, by definition,

$$\begin{aligned} \mu_{\mathcal{M}}^{\cup}(\mathbf{d}(S, T)) \times \mu_{\mathcal{M}}^{\cup}(\mathbf{d}U) &= \mu_{\mathcal{M}}^{|T|}(\mathbf{d}(S, T)) \times \mu_{\mathcal{M}}^{|U|}(\mathbf{d}U) \\ &= \mu_{\mathcal{M}}^{|T|+|U|}(\mathbf{d}(S, T, U)) \\ &= \mu_{\mathcal{M}}^{\cup}(\mathbf{d}(S, T, U)). \end{aligned}$$

Comparing with Equation (5), and noting that $|U_i|$ is the number of self-transitions in interval (t_{i-1}, t_i) , we see both are equal whenever U_S is compatible with $(s_0, S, T, U_{\mathcal{T}})$. The probability density at any incompatible setting of U_S is zero, giving us the desired result. \blacksquare

We can now incorporate the likelihoods coming from the observations X . Firstly, note that by assumption, X depends only on the MJP trajectory (s_0, S, T) and not on the auxiliary jumps U . Thus, the conditional distribution of $U_{\mathcal{T}}$ given (s_0, S, T, X) is still the inhomogeneous Poisson process given above. Let $X_{[w_i, w_{i+1})}$ represent the observations in the interval $[w_i, w_{i+1})$ (taking $w_{|W|+1} = t_{end}$). Throughout this interval, the MJP is in state v_i , giving a likelihood term:

$$L_i(v_i) = p(X_{[w_i, w_{i+1})} | \mathbf{S}(t) = v_i \text{ for } t \in [w_i, w_{i+1})). \quad (7)$$

For the case of noisy observations of the MJP state at a discrete set of times T^o , this simplifies to

$$L_i(v_i) = \prod_{j: t_j^o \in [w_i, w_{i+1})} p(X_{t_j^o} | \mathbf{S}(t_j^o) = v_i).$$

Conditioned on the times W , (s_0, V) is a Markov chain with initial distribution π_0 , transition matrix B and likelihoods given by Equation (7). We can efficiently resample (s_0, V) using the standard forward filtering-backward sampling (FFBS) algorithm. We provide a description of this algorithm in Appendix A. This cost of such a resampling step is $O(N^2|V|)$, quadratic in the number of states and linear in the length of the chain. Further, any structure in A (e.g., sparsity) is inherited by B and can be exploited easily. Let (\tilde{s}_0, \tilde{V}) be the new state sequence. Then $(\tilde{s}_0, \tilde{V}, W)$ will correspond to a new MJP path $\tilde{\mathbf{S}}(t) \equiv (\tilde{s}_0, \tilde{S}, \tilde{T})$, obtained by discarding virtual jumps from (\tilde{V}, W) . Effectively, given an MJP path, an iteration of our algorithm corresponds to introducing thinned events, re-labelling the thinned and actual transitions using FFBS, and then discarding the new thinned events to obtain a new MJP. We summarize this in Algorithm 2.

Algorithm 2 Blocked Gibbs sampler for an MJP on the interval $[t_{start}, t_{end}]$

Input: A set of observations X , and parameters A (the rate matrix), π_0 (the initial distribution over states) and $\Omega > \max_s(|A_s|)$.

The previous MJP path, $\mathbf{S}(t) \equiv (s_0, S, T)$.

Output: A new MJP trajectory $\tilde{\mathbf{S}}(t) \equiv (\tilde{s}_0, \tilde{S}, \tilde{T})$.

1: Sample $U_{\mathcal{T}} \subset [t_{start}, t_{end}]$ from a Poisson process with piecewise-constant rate

$$R(t) = (\Omega + A_{\mathbf{S}(t)}).$$

Define $W = T \cup U_{\mathcal{T}}$ (in increasing order).

2: Sample a path (\tilde{s}_0, \tilde{V}) from a discrete-time Markov chain with $1 + |W|$ steps using the FFBS algorithm. The transition matrix of the Markov chain is $B = (I + \frac{A}{\Omega})$ while the initial distribution over states is π_0 . The likelihood of state s at step i is

$$L_i(s) = p(X_{[w_i, w_{i+1})} | \mathbf{S}(t) = s \text{ for } t \in [w_i, w_{i+1})).$$

3: Let \tilde{T} be the set of times in W when the Markov chain changes state. Define \tilde{S} as the corresponding set of state values. **Return** $(\tilde{s}_0, \tilde{S}, \tilde{T})$.

Proposition 3 *The auxiliary variable Gibbs sampler described above has the posterior distribution $p(s_0, S, T | X)$ as its stationary distribution. Moreover, if $\Omega > \max_s |A_s|$, the resulting Markov chain is irreducible.*

Proof The first statement follows since the algorithm simply introduces auxiliary variables U , and then conditionally samples V given X and W . For the second, note that if $\Omega > \max_s(|A_s|)$, then the intensity of the subordinating Poisson process is strictly positive. Thus, there is positive probability density of sampling appropriate auxiliary jump times U and moving from any MJP trajectory to any other. ■

Note that it is essential for Ω to be strictly greater than $\max_s |A_s|$; equality is not sufficient for irreducibility. For example, if all diagonal elements of A are equal to Ω , then the Poisson process for $U_{\mathcal{T}}$ will have intensity 0, so that the set of jump times T will never increase.

Since FFBS returns a new state sequence \tilde{V} that is independent of V given W , the only dependence between successive MCMC samples arises because the new candidate jump times include the old jump times i.e., $T \subset W$. This means that the new MJP trajectory has non-zero probability of making a jump at a same time as the old trajectory. Increasing Ω introduces more virtual jumps, and as T becomes a smaller subset of W , we get faster mixing. Of course, increasing Ω makes the HMM chain grow longer, leading to a linear increase in the computational cost per iteration. Thus the parameter Ω allows a trade-off between mixing rate and computational cost. We will study this trade-off in Section 3.5. In all other experiments, we set $\Omega = \max_s(2|A_s|)$ as we find this works quite well, with the samplers typically converging after fewer than 5 iterations.

3.3 Previous Posterior Sampling Schemes

A simple approach when the MJP state is observed at the ends of an interval is rejection sampling: sample paths given the observed start state via Gillespie's algorithm, and reject those that do not end

in the observed end state (Nielsen, 2002). We can extend this to noisy observations by importance sampling or particle filtering (Fan and Shelton, 2008). Recently, Golightly and Wilkinson (2011) have applied particle MCMC methods to correct the bias introduced by standard particle filtering methods. However, these methods are efficient only in situations where the data exerts a relatively weak influence on the unobserved trajectory (compared to the prior): a large state-space or an unlikely end state can result in a large number of rejections or small effective sample sizes (Hobolth and Stone, 2009).

A second approach, more specific to MJPs, integrates out the infinitely many paths of the MJP in between observations using matrix exponentiation (Equation (1)), and uses forward-backward dynamic programming to sum over the states at the finitely many observation times (see Hobolth and Stone (2009) for a review). Unfortunately, matrix exponentiation is an expensive operation that scales as $O(N^3)$, cubically in the number of states. Moreover, the matrix resulting from matrix exponentiation is dense and any structure (like sparsity), in the rate matrix A cannot be exploited.

A third approach is, like ours, based on the idea of uniformization (Hobolth and Stone, 2009). This proceeds by producing independent posterior samples of the Poisson events W in the interval between observations, and then (like our sampler) running a discrete-time Markov chain on this set of times to sample a new trajectory. However, sampling from the posterior distribution over W is not easy, depending crucially on the observation process, and usually requires a random number of $O(N^3)$ matrix multiplications (as the sampler iterates over the possible number of Poisson events). By contrast, instead of producing independent samples, ours is an MCMC algorithm. At the price of producing dependent samples, our method scales as $O(N^2)$ given a random discretization of time, does not require matrix exponentiations, easily exploits structure in the rate matrix and naturally extends to various extensions of MJPs. Moreover, we demonstrate that our sampler mixes very rapidly. We point out here that as the number of states N increases, if the transition rates $A_{ss'}$, $s \neq s'$, remain $O(1)$, then the uniformization rate Ω and the total number of state transitions are $O(N)$. Thus, our algorithm now scales overall as $O(N^3)$, while the matrix exponentiation-based approach is $O(N^4)$. In either case, whether $A_{ss'}$ is $O(1)$ or $O(1/N)$, our algorithm is an order of magnitude faster.

3.4 Bayesian Inference on the MJP Parameters

In this section we briefly describe how full Bayesian analysis can be performed by placing priors on the MJP parameters A and π_0 and sampling them as part of the MCMC algorithm. Like Fearnhead and Sherlock (2006), we place independent gamma priors on the (negative) diagonal elements of A and independent Dirichlet priors on the transition probabilities. In particular, for all s let $p_{s's} = A_{s's}/|A_s|$ and define the prior:

$$|A_s| \sim \text{Gamma}(\alpha_1, \alpha_2),$$

$$(p_{s's}, s' \neq s) \sim \text{Dirichlet}(\beta).$$

This prior is conjugate, with sufficient statistics for the posterior distribution given a trajectory $\mathbf{S}(t)$ being the total amount of time T_s spent in each state s and the number of transitions $n_{s's}$ from each s to s' . In particular,

$$|A_s| | (s_0, \mathbf{S}, T) \sim \text{Gamma}(\alpha_1 + \sum_{s' \neq s} n_{s's}, \alpha_2 + T_s), \quad \text{and} \quad (8)$$

$$(p_{s's}, s' \neq s) | (s_0, \mathbf{S}, T) \sim \text{Dirichlet}(\beta + (n_{s's}, s' \neq s)) \quad (9)$$

It is important to note that we resample the rate matrix A conditioned on (s_0, S, T) , and *not* (v_0, V, W) . A new rate matrix \tilde{A} implies a new uniformization rate $\tilde{\Omega}$, and in the latter case, we must also account for the probability of the Poisson events W under $\tilde{\Omega}$. Besides being more complicated, this coupling between W and Ω can slow down mixing of the MCMC sampler. Thus, we first discard the thinned events U , update A conditioned only on the MJP trajectory, and then reintroduce the thinned events under the new parameters. We can view the sampler of Algorithm 2 as a transition kernel $\mathcal{K}_A((s_0, S, T), (\tilde{s}_0, \tilde{S}, \tilde{T}))$ that preserves the posterior distribution under the rate matrix A . Our overall sampler then alternately updates (s_0, S, T) via the transition kernel $\mathcal{K}_A(\cdot, \cdot)$, and then updates A given (s_0, S, T) .

Finally, we can either fix π_0 or (as is sometimes appropriate) set it equal to the stationary distribution of the MJP with rate matrix A . In the latter case, Equations (8) and (9) serve as a Metropolis-Hastings proposal. We accept a proposed \tilde{A} sampled from this distribution with probability equal to the probability of the current initial state under the stationary distribution of \tilde{A} . Note that computing this stationary distribution requires solving an $O(N^3)$ eigenvector problem, so that in this case, the overall Gibbs sampler scales cubically even though Algorithm 2 scales quadratically.

3.5 Experiments

We first look at the effect of the parameter Ω on the mixing on the MCMC sampler. We generated a random 5-by-5 matrix A (with hyperparameters $\alpha_1 = \alpha_2 = \beta = 1$), and used this to generate an MJP trajectory with a uniform initial distribution over states. The state of this MJP trajectory was observed via a Poisson process likelihood model (see Section 4), and posterior samples given the observations and A were produced by a C++ implementation of our algorithm. 1000 MCMC runs were performed, each run consisting of 10000 iterations after a burn-in of 1000 iterations. For each run, the number of transitions as well as the time spent in each state was calculated, and effective sample sizes (ESSs) of these statistics (the number of independent samples with the same ‘information’ as the correlated MCMC samples) were calculated using R-CODA (Plummer et al., 2006). The overall ESS of a run is defined to be the median ESS across all these ESSs.

Figure 3 (left) plots the overall ESS against computation time per run, for different scalings k , where $\Omega = k \max_s |A_s|$. We see that increasing Ω does increase the mixing rate, however the added computational cost quickly swamps out any benefit this might afford. Figure 3 (right) is a similar plot for the case where we also performed Bayesian inference for the MJP parameter A as described in Section 3.4. Now we estimated the ESS of all off-diagonal elements of the matrix A , and the overall ESS of an MCMC run is defined as the median ESS. Interestingly, in this scenario, the ESS is fairly insensitive to Ω , suggesting an ‘MCMC within Gibbs’ update as proposed here using dependent trajectories is as effective as one using independent trajectories. We found this to be true in general: when embedded within an outer MCMC sampler, our sampler produced similar effective ESSs as an MJP sampler that produces independent trajectories. The latter is typically more expensive, and in any case, we will show that the computational savings provided by our sampler far outweigh the cost of dependent trajectories.

In light of Figure 3, for all subsequent experiments we set $\Omega = 2 \max_s |A_s|$. Figure 4 shows the initial burn-in of a sampler with this setting for different initializations. The vertical axis shows the number of state transitions in the MJP trajectory of each iteration. This quantity quickly reaches its equilibrium value within a few iterations.

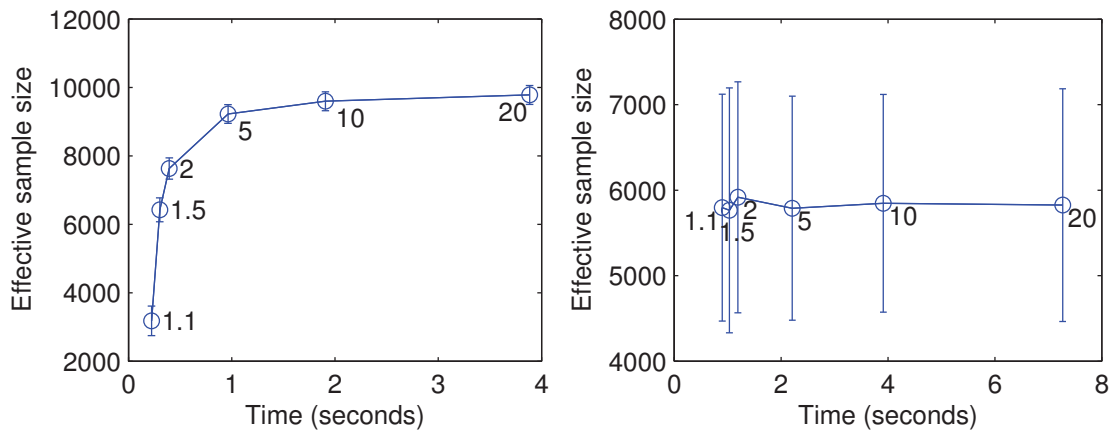


Figure 3: Effective sample sizes vs computation times for different scalings of Ω for (left) a fixed rate matrix A and (right) Bayesian inference on A . Whiskers are quartiles over 1000 runs.

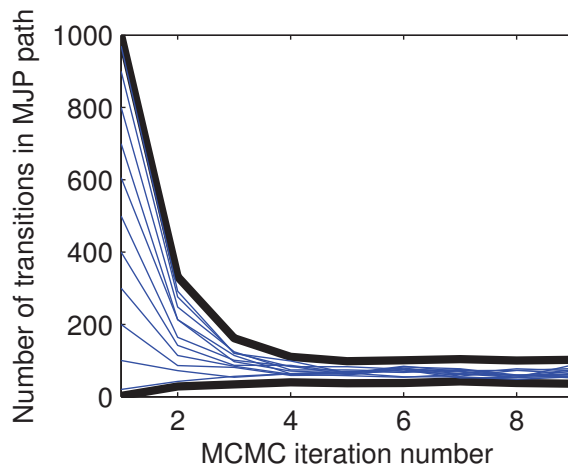


Figure 4: Trace plot of the number of MJP transitions for different initializations. Black lines are the maximum and minimum number of MJP transitions for each iteration, over all initializations.

4. Markov-Modulated Poisson Processes

A Markov modulated Poisson process (MMPP) is a doubly-stochastic Poisson process whose intensity function is piecewise-constant and distributed according to a Markov jump process. Suppose the MJP $(\mathbf{S}(t), t \in [t_{start}, t_{end}])$ has N states, and is parametrized by an initial distribution over states π_0 and a rate matrix A . Associate with each state s a nonnegative constant λ_s called the emission rate of state s . Let O be a set of points drawn from a Poisson process with piecewise-constant rate $R(t) = \lambda_{\mathbf{S}(t)}$. Note that O is unrelated to the subordinating Poisson process from the uniformization-based construction of the MJP, and we call it the output Poisson process. The Poisson observations O effectively form a continuous-time observation of the latent MJP, with the *absence* of Poisson events also informative about the MJP state. MMPPs have been used to model phenomenon like the distribution of rare DNA motifs along a gene (Fearhead and Sherlock, 2006), photon arrival in

single molecule fluorescence experiments (Burzykowski et al., 2003), and requests to web servers (Scott and Smyth, 2003).

Fearnhead and Sherlock (2006) developed an exact sampler for MMPPs based on a dynamic program for calculating the probability of O marginalizing out the MJP trajectory. The dynamic program keeps track of the probability of the MMPP emitting all Poisson events prior to a time t and ending in MJP state s . The dynamic program then proceeds by iterating over all Poisson events in O in increasing order, at each iteration updating probabilities using matrix exponentiation. A backward sampling step then draws an exact posterior sample of the MJP trajectory $(\mathbf{S}(t), t \in O)$ evaluated at the times in O . Finally a uniformization-based endpoint conditioned MJP sampler is used to fill in the MJP trajectory between every pair of times in O .

The main advantage of this method is that it produces independent posterior samples. It does this at the price of being fairly complicated and computationally intensive. Moreover, it has the disadvantage of operating at the time scale of the Poisson observations rather than the dynamics of the latent MJP. For high Poisson rates, the number of matrix exponentiations will be high even if the underlying MJP has very low transition rates. This can lead to an inefficient algorithm.

Our MCMC sampler outlined in the previous section can be straightforwardly extended to the MMPP without any of these disadvantages. Resampling the auxiliary jump events (step 1 in algorithm 2) remains unaffected, since conditioned on the current MJP trajectory, they are independent of the observations O . Step 2 requires calculating the emission likelihoods $L_i(s)$, which is simply given by:

$$L_i(s) = (\lambda_s)^{|O_i|} \exp(-\lambda_s(w_{i+1} - w_i)),$$

$|O_i|$ being the number of events of O in the interval $[w_i, w_{i+1})$. Note that evaluating this likelihood only requires counting the number of observed Poisson events between every successive pair of times in W . Compared to our algorithm, the approach of Fearnhead and Sherlock (2006) is much more involved and inefficient.

4.1 Experiments

In the following, we compare a C++ implementation of our algorithm with an implementation² of the algorithm of Fearnhead and Sherlock (2006), coded in C. We performed fully Bayesian inference, sampling both the MJP parameters (as described in Section 3.4) and the Poisson rates λ_s (conjugate gamma priors were placed on these). In all instances, our algorithm did significantly better, the performance improvement increasing with the complexity of the problem.

In the first set of experiments, the dimension of the latent MJP was fixed to 5. The prior on the rate matrix A had parameters $\alpha_1 = \alpha_2 = \beta = 1$ (see Section 3.4). The shape parameter of the gamma prior on the emission rate of state s , λ_s , was set to s (thereby breaking symmetry across states); the scale parameter was fixed at 1. 10 draws of O were simulated using the MMPP. For each observed O , both MCMC algorithms were run for 1000 burn-in iterations followed by 10000 iterations where samples were collected. For each run, the ESS for each parameter was estimated using R-CODA, and the overall ESS was defined to be the median ESS over all parameters.

Figure 5 reports the average computation times required by each algorithm to produce 100 effective samples, under different scenarios. The leftmost plot shows the computation times as a function of the numbers of Poisson events observed in an interval of fixed length 10. For our

². Code was downloaded from Chris Sherlock’s webpage.

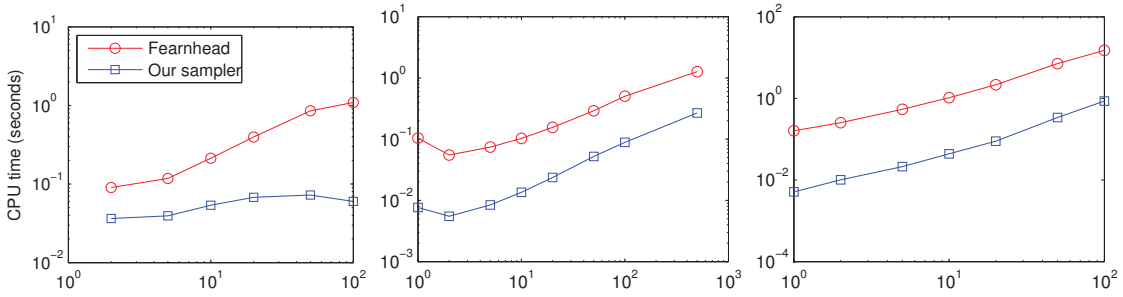


Figure 5: CPU time to produce 100 effective samples as we observe (left) increasing number of Poisson events in an interval of length 10, (centre) 10 Poisson events over increasing time intervals, and (right) increasing intervals with the number of events increasing on average.

sampler, increasing the number of observed events leaves the computation time largely unaffected, while for the sampler of Fearnhead and Sherlock (2006), this increases quite significantly. This reiterates the point that our sampler works at the time scale of the latent MJP, while Fearnhead and Sherlock (2006) work at the time scale of the observed Poisson process. In the middle plot, we fix the number of observed Poisson events to 10, while increasing the length of the observation interval instead, while in the rightmost plot, we increase both the interval length and the average number of observations in that interval. In both cases, our sampler again offers increased efficiency of up to two orders of magnitude. In fact, the only problems where we observed the sampler of Fearnhead and Sherlock (2006) to outperform ours were low-dimensional problems with only a few Poisson observations in a long interval, and with one very unstable state. A few very stable MJP states and a few very unstable ones results in a high uniformization rate Ω but only a few state transitions. The resulting large number of virtual jumps can make our sampler inefficient.

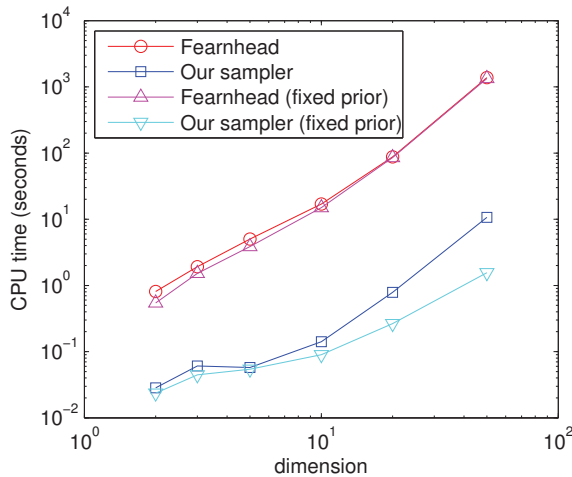


Figure 6: CPU time to produce 100 effective samples as the MJP dimension increases

In Figure 6, we plot the time to produce 100 effective samples as the number of states of the latent MJP increases. Here, we fixed the number of Poisson observations to 10 over an interval

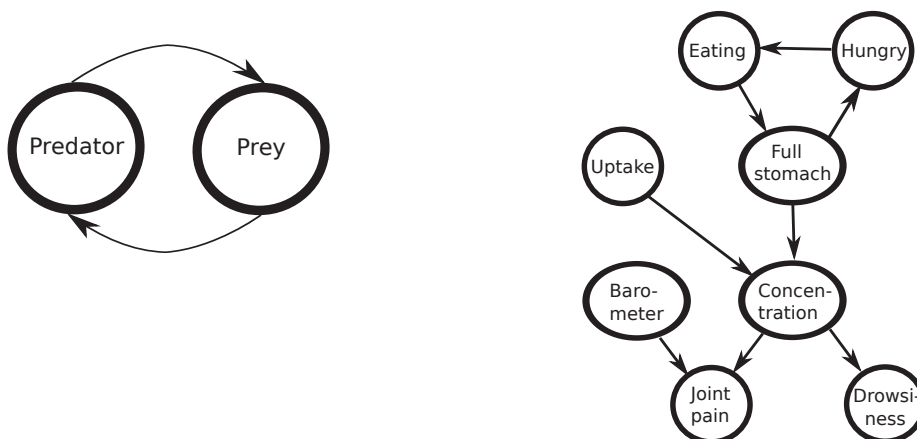


Figure 7: The predator-prey network (left) and the drug-effect CTBN (right)

of length 10. We see that our sampler (plotted with squares) offers substantial speed-up over the sampler of Fearnhead and Sherlock (2006) (plotted with circles). We see that for both samplers computation time scales cubically with the latent dimension. However, recall that this cubic scaling is not a property of our MJP trajectory sampler; rather it is a consequence of using the equilibrium distribution of a sampled rate matrix as the initial distribution over states, which requires calculating an eigenvector of a proposed rate matrix. If we fix the initial distribution over states (to the discrete uniform distribution), giving the line plotted with inverted triangles in the figure, we observe that our sampler scales quadratically.

5. Continuous-Time Bayesian Networks (CTBNs)

Continuous-time Bayesian networks (CTBNs) are compact, multi-component representations of MJPs with structured rate matrices (Nodelman et al., 2002). Special instances of these models have long existed in the literature, particularly stochastic kinetic models like the Lotka-Volterra equations, which describe interacting populations of animal species, chemical reactants or gene regulatory networks (Wilkinson, 2009). There have also been a number of related developments, see for example Bolch et al. (1998) or Didelez (2008). For concreteness however, we shall focus on CTBNs, a formalism introduced in Nodelman et al. (2002) to harness the representational power of Bayesian networks to characterize structured MJPs.

Just as the familiar Bayesian network uses a product of conditional probability tables to represent a much larger probability table, so too a CTBN represents a structured rate matrix with smaller conditional rate matrices. An m -component CTBN represents the state of an MJP at time t with the states of m nodes $\mathbf{S}^1(t), \dots, \mathbf{S}^m(t)$ in a directed (and possibly cyclic) graph \mathcal{G} . Figure 7 shows two CTBNs, the ‘predator-prey network’ and the ‘drug-effect network’. The former is a CTBN governed by the Lotka-Volterra equations (see subsection 5.3.1), while the latter is used to model the dependencies in events leading to and following a patient taking a drug (Nodelman et al., 2002).

Intuitively, each node of the CTBN acts as an MJP with an instantaneous rate matrix that depends on the current configuration of its parents (and not its children, although the presence of directed cycles means a child can be a parent as well). The trajectories of all nodes are piecewise

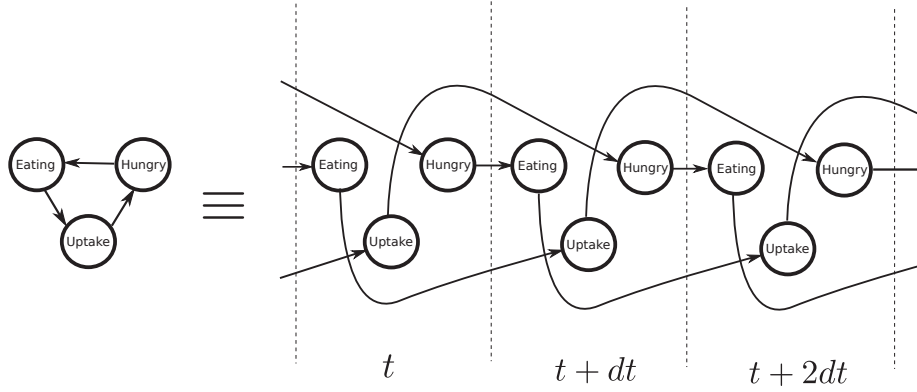


Figure 8: Expanded CTBN

constant, and when a node changes state, the event rates of all its children change. The graph \mathcal{G} and the set of rate matrices (one for each node and for each configuration of its parents) characterize the dynamics of the CTBN, the former describing the structure of the dependencies between various components, and the latter quantifying this. Completing the specification of the CTBN is an initial distribution π_0 over the state of nodes, possibly specified via a Bayesian network.

It is convenient to think of a CTBN as a compact representation of an expanded (and now acyclic) graph, consisting of the nodes of \mathcal{G} repeated infinitely along a continuum (viz. time). In this graph, arrows lead from a node at a time t to instances of its children at time $t + dt$. Figure 8 displays this for a section of the drug-effect CTBN. The rates associated with a particular node at time $t + dt$ are determined by the configuration of its parents at time t . Figure 8 is the continuous-time limit of a class of discrete-time models called dynamic Bayesian networks (DBNs) (Murphy, 2002). In a DBN, the state of a node at stage $i + 1$ is dependent upon the configuration of its parents at stage i . Just as MJPs are continuous-time limits of discrete-time Markov chains, CTBNs are also continuous-time limits of DBNs.

It is possible to combine all local rate matrices of a CTBN into one global rate matrix (see Nodelman et al., 2002), resulting in a simple MJP whose state-space is the product state-space of all component nodes. Consequently, it is possible, conceptually at least, to directly sample a trajectory over an interval $[t_{start}, t_{end}]$ using Gillespie's algorithm. However, with an eye towards inference, Algorithm 3 describes a generative process that exploits the structure in the graph \mathcal{G} . Like Section 2, we represent the trajectory of the CTBN, $\mathbf{S}(t)$, with the initial state s_0 and the pair of sequences (S, T) . Let the CTBN have m nodes. Now, s_i , the i th element of S , is an m -component vector representing the states of all nodes at t_i , the time of the i th state change of the CTBN. We write this as $s_i = (s_i^1, \dots, s_i^m)$. Let k_i identify the component of the CTBN that changed state at t_i . The rate matrix of a node n varies over time as the configuration of its parents changes, and we will write $A^{n,t}$ for the relevant matrix at time t . Following Equation (2), we can write down the probability density of (s_0, S, T) as

$$p(s_0, S, T) = \pi_0(s_0) \left(\prod_{i=1}^{|T|} A_{s_i s_{i-1}}^{k_i, t_i} \right) \exp \left(- \sum_{k=1}^m \int_{t_{start}}^{t_{end}} |A_{\mathbf{S}^k(t)}^{k,t}| dt \right). \quad (10)$$

Algorithm 3 Algorithm to sample a CTBN trajectory on the interval $[t_{start}, t_{end}]$

Input: The CTBN graph \mathcal{G} , a set of rate matrices $\{A\}$ for all nodes and for all parent configurations and an initial distribution over states π_0 .
Output: A CTBN trajectory $\mathbf{S}(t) \equiv (s_0, S, T)$.

- 1: Draw an initial configuration $s_0 \equiv (s_0^1, s_0^2, \dots) \sim \pi_0$. Set $t_0 = t_{start}$ and $i = 0$.
 - 2: **loop**
 - 3: For each node k , draw $z^k \sim \exp(|A_{s_i^k}^{k, t_i}|)$.
 - 4: Let $k_{i+1} = \operatorname{argmin}_k z^k$ be the first node to change state.
 - 5: **If** $t_i + z^{k_{i+1}} > t_{end}$ **then return** $(s_0, \dots, s_i, t_1, \dots, t_i)$ **and stop**.
 - 6: Increment i and let $t_i = t_{i-1} + z^{k_i}$ be the next jump time.
 - 7: Let $s' = s_{i-1}^{k_i}$ be the previous state of node k_i .
 - 8: Set $s_i^{k_i} = s$ with probability proportional to $A_{ss'}^{k_i, t_{i-1}}$ for each $s \neq s'$.
 - 9: Set $s_i^k = s_{i-1}^k$ for all $k \neq k_i$.
 - 10: **end loop**
-

5.1 Inference in CTBNs

We now consider the problem of posterior inference over trajectories given some observations. Write the parents and children of a node k as $\mathcal{P}(k)$ and $\mathcal{C}(k)$ respectively. Let $\mathcal{MB}(k)$ be the Markov blanket of node k , which consists of its parents, children, and the parents of its children. Given the entire trajectories of all nodes in $\mathcal{MB}(k)$, node k is independent of all other nodes in the network (Nodelman et al., 2002) (see also Equation (12) below). This suggests a Gibbs sampling scheme where the trajectory of each node is resampled given the configuration of its Markov blanket. This approach was followed by El-Hay et al. (2008).

However, even without any associated observations, sampling a node trajectory conditioned on the complete trajectory of its Markov blanket is not straightforward. To see this, rearrange the terms of Equation (10) to give

$$p(s_0, S, T) = \pi_0(s_0) \prod_{k=1}^m \phi(S^k, T^k | s_0, S^{\mathcal{P}(k)}, T^{\mathcal{P}(k)}), \quad \text{and}$$

$$\phi(S^k, T^k | s_0, S^{\mathcal{P}(k)}, T^{\mathcal{P}(k)}) = \left(\prod_{i: k_i=k} A_{s_i^k s_{i-1}^k}^{k, t_i} \right) \exp \left(- \int_{t_{start}}^{t_{end}} |A_{\mathbf{S}^k(t)}^{k, t}| dt \right), \quad (11)$$

where for any set of nodes B , (s_0^B, S^B, T^B) represents the associated trajectories. Note that the $\phi(\cdot)$ terms are not conditional densities given parent trajectories, since the graph \mathcal{G} can be cyclic. We must also account for the trajectories of node k 's children, so that the conditional density of (s_0^k, S^k, T^k) is actually

$$p(s_0^k, S^k, T^k | s_0^{-k}, S^{-k}, T^{-k}) \propto \pi_0(s_0^k | s_0^{-k}) \phi(S^k, T^k | s_0, S^{\mathcal{P}(k)}, T^{\mathcal{P}(k)}) \cdot \prod_{c \in \mathcal{C}(k)} \phi(S^c, T^c | s_0, S^{\mathcal{P}(c)}, T^{\mathcal{P}(c)}). \quad (12)$$

Here $-k$ denotes all nodes other than k . Thus, even over an interval of time where the parent configuration remains constant, the conditional distribution of the trajectory of a node is not a homogeneous

MJP because of the effect of the node’s children, which act as ‘observations’ that are continuously observed. For any child c , if $A^{c,t}$ is constant over t , the corresponding $\phi(\cdot)$ is the density of an MJP given the initial state. Since $A^{c,t}$ varies in a piecewise-constant manner according to the state of k , the $\phi(\cdot)$ term is actually the density of a piecewise-inhomogeneous MJP. Effectively, we have a ‘MJP-modulated MJP’, so that the inference problem here is a generalization of that for the MMPP of Section 4.

El-Hay et al. (2008) described a matrix-exponentiation-based algorithm to update the trajectory of node k . At a high-level their algorithm is similar to Fearnhead and Sherlock (2006) for MMPPs, with the Poisson observations of the MMPP generalized to transitions in the trajectories of child nodes. Consequently, it uses an expensive forward-backward algorithm involving matrix exponentiations. In addition, El-Hay et al. (2008) resort to discretizing time via a binary search to obtain the transition times upto machine accuracy.

5.2 Auxiliary Variable Gibbs Sampling for CTBNs

We now show how our uniformization-based sampler can easily be adapted to conditionally sample a trajectory for node k without resorting to approximations. In the following, for notational simplicity, we will drop the superscript k whenever it is clear from context. For node k , the MJP trajectory (s_0, \mathcal{S}, T) has a uniformized construction from a subordinating Poisson process. The piecewise constant trajectories of the parents of k imply that the MJP is piecewise homogeneous, and we will use a piecewise constant rate Ω^t which dominates the associated transition rates, i.e., $\Omega^t > |A_s^{k,t}|$ for all s . This allows the dominating rate to ‘adapt’ to the local transition rates, and is more efficient when, e.g., the transition rates associated with different parent configurations are markedly different. Recall also that our algorithm first reconstructs the thinned Poisson events $U_{\mathcal{T}}$ using a piecewise homogeneous Poisson process with rate $(\Omega^t + A_{\mathcal{S}(t)}^{k,t})$, and then updates the trajectory using the forward-backward algorithm (so that $W = T \cup U_{\mathcal{T}}$ forms the candidate transitions times of the MJP).

In the present CTBN context, just as the subordinating Poisson process is inhomogeneous, so too the Markov chain used for the forward-backward algorithm will have different transition matrices at different times. In particular, the transition matrix at a time w_i (where $W = (w_1, \dots, w_{|W|})$) is

$$B_i = I + \frac{A^{k,w_i}}{\Omega^{w_i}}.$$

Finally, we need also to specify the likelihood function $L_i(s)$ accounting for the trajectories of the children in addition to actual observations in each time interval $[w_i, w_{i+1})$. From Equations (11) and (12), this is given by

$$L_i(s) = L_i^O(s) \prod_{c \in C(k)} \left(\prod_{j: k_j = k, t_j \in [w_i, w_{i+1})} A_{s_{j-1}^{k_j, k}}^{k, t_j} \right) \exp \left(- \int_{w_i}^{w_{i+1}} |A_{\mathcal{S}^k(t)}^{k,t}| dt \right),$$

where $L_i^O(s)$ is the likelihood coming from actual observations dependent on the state of node k in the time interval. Note that the likelihood above depends only on the number of transitions each of the children make as well as how much time they spend in each state, for each parent configuration.

The new trajectory $\tilde{\mathcal{S}}^k(t)$ is now obtained using the forward-filtering backward-sampling algorithm, with the given inhomogeneous transition matrices and likelihood functions. The following proposition now follows directly from our previous results in Section 3:

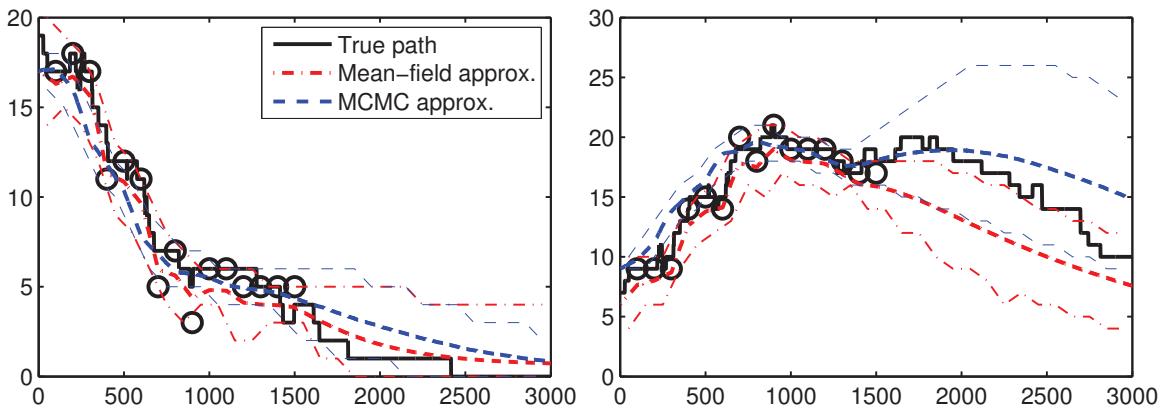


Figure 9: Posterior (mean and 90% credible intervals) over (left) prey and (right) predator paths (observations (circles) were available only until 1500).

Proposition 4 *The auxiliary variable Gibbs sampler described above converges to the posterior distribution over the CTBN sample paths.*

Note that our algorithm produces a new trajectory that is dependent, through T , on the previous trajectory (unlike a true Gibbs update as in El-Hay et al. (2008) where they are independent). However, we find that since the update is part of an overall Gibbs cycle over nodes of the CTBN, the mixing rate is actually dominated by dependence across nodes. Thus, a true Gibbs update has negligible benefit towards mixing, while being more expensive computationally.

5.3 Experiments

In the following, we evaluate a C++ implementation of our algorithm on a number of CTBNs. As before, the dominating rate Ω^t was set to $\max_s 2|A_s^{k,t}|$.

5.3.1 THE LOTKA-VOLTERRA PROCESS

We first apply our sampler to the Lotka-Volterra process (Wilkinson, 2009; Opper and Sanguinetti, 2007). Commonly referred to as the predator-prey model, this describes the evolution of two interacting populations of ‘prey’ and ‘predator’ species. The two species form the two nodes of a cyclic CTBN (Figure 7 (left)), whose states x and y represent the sizes of the prey and predator populations. The process rates are given by

$$\begin{aligned} A(\{x, y\} \rightarrow \{x+1, y\}) &= \alpha x, & A(\{x, y\} \rightarrow \{x-1, y\}) &= \beta xy, \\ A(\{x, y\} \rightarrow \{x, y+1\}) &= \delta xy, & A(\{x, y\} \rightarrow \{x, y-1\}) &= \gamma y, \end{aligned}$$

where we set the parameters as follows: $\alpha = 5 \times 10^{-4}$, $\beta = 1 \times 10^{-4}$, $\gamma = 5 \times 10^{-4}$, $\delta = 1 \times 10^{-4}$. All other rates are 0. This defines two infinite sets of infinite-dimensional conditional rate matrices. In its present form, our sampler cannot handle this infinite state-space (but see Rao and Teh, 2012). Like Opper and Sanguinetti (2007), we limit the maximum number of individuals of each species to 200, leaving us with 400 rate matrices of size 200×200 . Note that these matrices are tridiagonal and very sparse: at any time the size of each population can change by at most one. Consequently, the

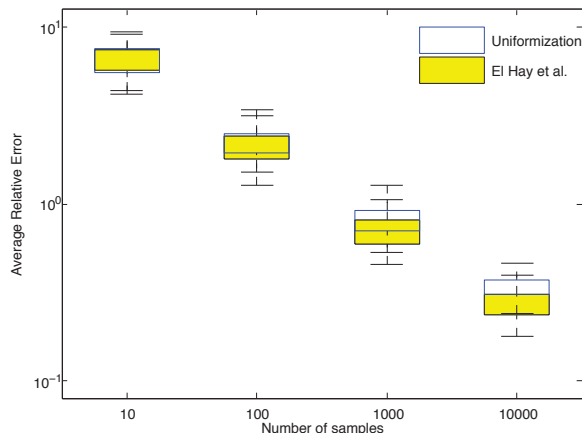


Figure 10: Average relative error vs number of samples for 1000 independent runs; burn-in = 200. Note that in this scenario, uniformization was about 12 times faster, so that for the same computational effort, it produces significantly lower errors.

complexity of our algorithm scales *linearly* with the number of states (we did not modify our code to exploit this structure, though this is straightforward). A ‘true’ path of predator-prey population sizes was sampled from this process, and its state at time $t = 0$ was observed noiselessly. Additionally 15 noisy observations were generated, spaced uniformly at intervals of 100. The noise process was:

$$p(X(t)|\mathbf{S}(t)) \propto \frac{1}{2^{|X(t)-\mathbf{S}(t)|} + 10^{-6}}.$$

Given these observations (as well as the true parameter values), we approximated the posterior distribution over paths by two methods: using 1000 samples from our MCMC sampler (with a burn-in period of 100) and using the mean-field (MF) approximation of Opper and Sanguinetti (2007)³. We could not apply the implementation of the Gibbs sampler of (El-Hay et al., 2008) (see Section 5.4) to a state-space and time-interval this large. Figure 9 shows the true paths (in black), the observations (as circles) as well as the posterior means and 90% credible intervals produced by the two algorithms for the prey (left) and predator (right) populations. As can be seen, both algorithms do well over the first half of the interval where data is present. In the second half, the MF algorithm appears to underestimate the predicted size of the predator population. On the other hand, the MCMC posterior reflects the true trajectory better. In general, we found the MF algorithm to underestimate the posterior variance in the MJP trajectories, especially over regions with few observations.

5.4 Average Relative Error vs Number of Samples

For the remaining experiments, we compared our sampler with the Gibbs sampler of El-Hay et al. (2008). For this comparison, we used the CTBN-RLE package of Shelton et al. (2010) (also implemented in C++). In all our experiments, as with the MMPP, we found our algorithm to be significantly faster, especially for larger problems. To prevent details of the two implementations from clouding the picture and to reiterate the benefit afforded by avoiding matrix exponentiations,

3. We thank Guido Sanguinetti for providing us with his code.

we also measured the amount of time CTBN-RLE spent exponentiating matrices. This constituted between 10% to 70% of the total running time of their algorithm. In the plots we refer to this as ‘El Hay et al. (Matrix Exp.)’. We found that our algorithm took less time than even this.

In our first experiment, we followed El-Hay et al. (2008) in studying how average relative error varies with the number of samples from the Markov chain. Average relative error is defined by $\sum_j \frac{|\hat{\theta}_j - \theta_j|}{\theta_j}$, and measures the total normalized difference between empirical ($\hat{\theta}_j$) and true (θ_j) averages of sufficient statistics of the posterior. The statistics in question are the time spent by each node in different states as well as the number of transitions from each state to the others. The exact values were calculated by numerical integration when possible, otherwise from a very long run of CTBN-RLE.

As in El-Hay et al. (2008), we consider a CTBN with the topology of a chain, consisting of 5 nodes, each with 5 states. The states of the nodes were observed at times 0 and 20 and we produced endpoint-conditioned posterior samples of paths over the time interval $[0, 20]$. We calculate the average relative error as a function of the number of samples, with a burn-in of 200 samples. Figure 10 shows the results from running 1000 independent chains for both samplers. Not surprisingly, the sampler of El-Hay et al. (2008), which produces conditionally independent samples, has slightly lower errors. However the difference in relative errors is minor, and is negligible when considering the dramatic (sometimes up to two orders of magnitude; see below) speed improvements of our algorithm. For instance, to produce the 10000 samples, the El-Hay et al. (2008) sampler took about 6 minutes, while our sampler ran in about 30 seconds.

5.5 Time Requirements for the Chain-Shaped CTBN

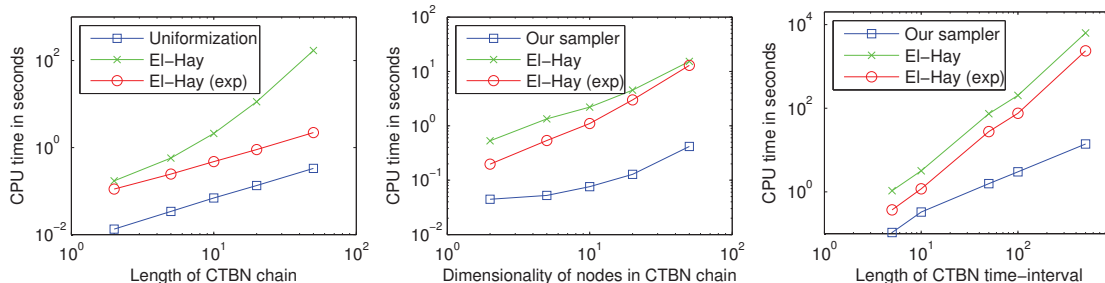


Figure 11: CPU time vs (left) length of CTBN chain (centre) number of states of CTBN nodes (right) time interval of CTBN paths.

In the next two experiments, we compare the times required by CTBN-RLE and our uniformization-based sampler to produce 100 effective samples as the size of the chain-shaped CTBN increased in different ways. In the first cases, we increased the length of the chain, and in the second, the dimensionality of each node. In both cases, we produced posterior samples from an endpoint-conditioned CTBN with random gamma distributed parameters.

The time requirements were estimated from runs of 10000 samples after a burn-in period of 1000 iterations. Since CTBN-RLE does not support Bayesian inference for CTBN parameters, we kept these fixed to the truth. To produce ESS estimates, we counted the number of transitions of

each node and the amount of time spent in each state, and for each MCMC run, we estimated the ESS of these quantities. Like in Section 4.1, the overall ESS is the median of these estimates. Each point in the figures is an average over 10 simulations.

In the first of these experiments, we measured the times to produce 100 effective samples for the chain-shaped CTBN described above, as the number of nodes in the chain (i.e., its length) increases. The leftmost plot in Figure 11 shows the results. As might be expected, the time required by our algorithm grows linearly with the number of nodes. For El-Hay et al. (2008), the cost of the algorithm grows faster than linear, and quickly becoming unmanageable. The time spent calculating matrix exponentials *does* grow linearly, however our uniformization-based sampler always takes less time than even this.

Next, we kept the length of the chain fixed at 5, instead increasing the number of states per node. As seen in the middle plot, once again, our sampler is always faster. Asymptotically, we expect our sampler to scale as $O(N^2)$ and El-Hay et al. (2008) as $O(N^3)$. While we have not hit that regime yet, we can see that the cost of our sampler grows more slowly with the number of states.

5.6 Time Requirements for the Drug-Effect CTBN

Our final experiment, reported in the rightmost plot of Figure 11, measures the time required as the interval length ($t_{end} - t_{start}$) increases. For this experiment, we used the drug-effect network shown in Figure 7, where the parameters were set to standard values (obtained from CTBN-RLE) and the state of the network was fully observed at the beginning and end times. Again, our algorithm is the faster of the two, showing a linear increase in computational costs with the length of the interval. It is worth pointing out here that the algorithm of El-Hay et al. (2008) has a ‘precision’ parameter, and that by reducing the desired temporal precision, faster performance can be obtained. However, since our sampler produces *exact* samples (up to numerical precision), our comparison is fair. In the above experiments, we left this parameter at its default value.

6. Discussion

We proposed a novel Markov chain Monte Carlo sampling method for Markov jump processes. Our method exploits the simplification of the structure of the MJP resulting from the introduction of auxiliary variables via the idea of uniformization. This constructs a Markov jump process by subordinating a Markov chain to a Poisson process, and amounts to running a Markov chain on a random discretization of time. Our sampler is a blocked Gibbs sampler in this augmented representation and proceeds by alternately resampling the discretization given the Markov chain and vice versa. Experimentally, we find that this auxiliary variable Gibbs sampler is computationally very efficient. The sampler easily generalizes to other MJP-based models, and we presented samplers for Markov-modulated Poisson processes and continuous-time Bayesian networks. In our experiments, we showed significant speed-up compared to state-of-the-art samplers for both.

Our method opens a number of avenues worth exploring. One concerns the subordinating Poisson rate Ω which acts as a free-parameter of the sampler. While our heuristic of setting this to $\max_s 2|A_s|$ worked well in our experiments, this may not be the case for rate matrices with widely varying transition rates. A possible approach is to ‘learn’ a good setting of this parameter via adaptive MCMC methods. More fundamentally, it would be interesting to investigate if theoretical claims can be made about the ‘best’ setting of this parameter under some measures of mixing speed and computational cost.

Next, there are a number of immediate generalizations of our sampler. First, our algorithm is easily applicable to inhomogeneous Markov jump processes where techniques based on matrix exponentiation cannot be applied. Following recent work (Rao and Teh, 2011b), we can also look at generalizing our sampler to semi-Markov processes where the holding times of the states follow non-exponential distributions. These models find applications in fields like biostatistics, neuroscience and queuing theory (Mode and Pickens, 1988). By combining our technique with slice sampling ideas (Neal, 2003), we can explore Markov jump processes with countably infinite state spaces. Another generalization concerns MJPs with unbounded rate matrices. For the predator-prey model, we avoided this problem by bounding the maximum population sizes; otherwise it is impossible to choose a dominating Ω . Of course, in practical settings, any trajectory from this process is bounded with probability 1, and we can extend our method to this case by treating Ω as a trajectory dependent random variable. For some work in this direction, we refer to Rao and Teh (2012).

Acknowledgments

This work was done while both authors were at the Gatsby Computational Neuroscience Unit, University College London. We would like to acknowledge the Gatsby Charitable Foundation for generous funding. We thank the associate editor and the anonymous reviewers for useful comments.

Appendix A. The Forward-Filtering Backward-Sampling (FFBS) Algorithm

For completeness, we include a description of the forward-filtering backward-sampling algorithm for discrete-time Markov chains. The earliest references for this that we are aware of are Fr \ddot{u} wirth-Schnatter (1994) and Carter and Kohn (1996).

Let S_t , $t \in \{0, \dots, T\}$ be a discrete-time Markov chain with a discrete state space $\mathcal{S} \equiv \{1, \dots, N\}$. We allow the chain to be inhomogeneous, with B^t being the state transition matrix at time t (so that $p(S_{t+1} = s' | S_t = s) = B^t_{s's}$). Let π_0 be the initial distribution over states at $t = 0$. Let O^t be a noisy observation of the state at time t , with the likelihood given by $L^t(s) = p(O^t | S^t = s)$. Given a set of observations $O = (O^0, \dots, O^T)$, FFBS returns an independent posterior sample of the state vector.

Define $\alpha^t(s) = p(O^0, \dots, O^{t-1}, S^t = s)$. From the Markov property, we have the following recursion:

$$\alpha^{t+1}(s') = \sum_{s=1}^N \alpha^t(s) L^t(s) B^t_{s's}.$$

Calculating this for all N values of s' takes $O(N^2)$ computation, and a forward pass through all T times is $O(TN^2)$. At the end of the forward pass, we have a vector

$$\beta^T(s) := L^T(s) \alpha^T(s) = p(O, S_T = s) \propto p(S_T = s | O).$$

It is easy to sample a realization of S_T from this. Next, note that

$$\begin{aligned} p(S_t = s | S_{t+1} = s', O) &\propto p(S_t = s, S_{t+1} = s', O) \\ &= \alpha^t(s) B^t_{s's} L^t(s) p(O^{t+1}, \dots, O^T | S_{t+1} = s') \\ &\propto \alpha^t(s) B^t_{s's} L^t(s), \end{aligned}$$

where the second equality follows from the Markov property. This too is easy to sample from, and the backward pass of FFBS successively samples S_{T-1} to S_0 . We thus have a sample (S_0, \dots, S_T) . The overall algorithm is given below:

Algorithm 4 The forward-filtering backward-sampling algorithm

Input: An initial distribution over states π_0 , a sequence of transition matrices B^t , a sequence of observations $O = (O_1, \dots, O_T)$ with likelihoods $L^t(s) = p(O^t | S^t = s)$.

Output: A realization of the Markov chain (S_0, \dots, S_T) .

- 1: Set $\alpha^0(s) = \pi_0(s)$.
 - 2: **for** $t = 1 \rightarrow T$ **do**
 - 3: $\alpha^t(s') = \sum_{s=1}^N (\alpha^{t-1}(s) L^{t-1}(s) B_{s's}^{t-1})$ for $s' \in \{1, \dots, N\}$.
 - 4: **end for**
 - 5: Sample $S_T \sim \beta^T(\cdot)$, where $\beta^T(s) := L^T(s) \alpha^T(s)$.
 - 6: **for** $t = T \rightarrow 0$ **do**
 - 7: Define $\beta^t(s) = \alpha^t(s) B_{S_{t+1}s}^t L^t(s)$.
 - 8: Sample $S_t \sim \beta^t(\cdot)$.
 - 9: **end for**
 - 10: **return** (S_0, \dots, S_T) .
-

References

- G. Bolch, S. Greiner, H. de Meer, and K. S. Trivedi. *Queueing Networks and Markov Chains: Modeling and Performance Evaluation with Computer Science Applications*. Wiley-Interscience, New York, NY, USA, 1998. ISBN 0-471-19366-6.
- R. J. Boys, D. J. Wilkinson, and T. B. L. Kirkwood. Bayesian inference for a discretely observed stochastic kinetic model. *Statistics and Computing*, 18(2):125–135, 2008.
- L. Breuer. *From Markov Jump Processes to Spatial Queues*. Springer, 2003. ISBN 978-1-4020-1104-7.
- T. Burzykowski, J. Szubiakowski, and T. Rydén. Analysis of photon count data from single-molecule fluorescence experiments. *Chemical Physics*, 288(2-3):291–307, 2003.
- C. K. Carter and R. Kohn. Markov chain Monte Carlo in conditionally Gaussian state space models. *Biometrika*, 83:589–601, 1996.
- E. Çinlar. *Introduction to Stochastic Processes*. Prentice Hall, 1975.
- I. Cohn, T. El-Hay, N. Friedman, and R. Kupferman. Mean field variational approximation for continuous-time Bayesian networks. *J. Mach. Learn. Res.*, 11:2745–2783, December 2010. ISSN 1532-4435.
- D. J. Daley and D. Vere-Jones. *An Introduction to the Theory of Point Processes*. Springer, 2008.
- V. Didelez. Graphical models for marked point processes based on local independence. *Journal of the Royal Statistical Society: Series B*, 70(1):245–264, 2008. ISSN 1467-9868.

- T. El-Hay, N. Friedman, and R. Kupferman. Gibbs sampling in factorized continuous-time Markov processes. In *Proceedings of the Twenty-fourth Conference on Uncertainty in Artificial Intelligence (UAI)*, pages 169–178, 2008.
- R. Elliott and C. Osakwe. Option pricing for pure jump processes with Markov switching compensators. *Finance and Stochastics*, 10:250–275, 2006.
- Y. Fan and C. R. Shelton. Sampling for approximate inference in continuous time Bayesian networks. In *Tenth International Symposium on Artificial Intelligence and Mathematics*, 2008.
- P. Fearnhead and C. Sherlock. An exact Gibbs sampler for the Markov-modulated Poisson process. *Journal Of The Royal Statistical Society Series B*, 68(5):767–784, 2006.
- S. Frühwirth-Schnatter. Data augmentation and dynamic linear models. *J. Time Ser. Anal.*, 15:183–202, 1994.
- D. T. Gillespie. Exact stochastic simulation of coupled chemical reactions. *J. Phys. Chem.*, 81(25):2340–2361, 1977. ISSN 0022-3654.
- A. Golightly and D. J. Wilkinson. Bayesian parameter inference for stochastic biochemical network models using particle Markov chain Monte Carlo. *Interface Focus*, 1(6):807–820, December 2011.
- A. Hobolth and E. A Stone. Simulation from endpoint-conditioned, continuous-time Markov chains on a finite state space, with applications to molecular evolution. *Ann. Appl. Stat.*, 3(3):1204, 2009. ISSN 1941-7330.
- A. Jensen. Markoff chains as an aid in the study of Markoff processes. *Skand. Aktuarietiedskr.*, 36:87–91, 1953.
- O. Kallenberg. *Foundations of Modern Probability*. Probability and its Applications. Springer-Verlag, New York, Second edition, 2002. ISBN 0-387-95313-2.
- C. J. Mode and G. T. Pickens. Computational methods for renewal theory and semi-Markov processes with illustrative examples. *The American Statistician*, 42(2):pp. 143–152, 1988. ISSN 00031305.
- K. P. Murphy. *Dynamic Bayesian Networks: Representation, Inference and Learning*. PhD thesis, University of California, Berkeley, 2002.
- R. M. Neal. Slice sampling. *Annals of Statistics*, 31:705–767, 2003.
- R. Nielsen. Mapping mutations on phylogenies. *Syst Biol*, 51(5):729–739, 2002.
- U. Nodelman, C.R. Shelton, and D. Koller. Continuous time Bayesian networks. In *Proceedings of the Eighteenth Conference on Uncertainty in Artificial Intelligence (UAI)*, pages 378–387, 2002.
- U. Nodelman, D. Koller, and C.R. Shelton. Expectation propagation for continuous time Bayesian networks. In *Proceedings of the Twenty-first Conference on Uncertainty in Artificial Intelligence (UAI)*, pages 431–440, July 2005.

- M. Opper and G. Sanguinetti. Variational inference for Markov jump processes. In *Advances in Neural Information Processing Systems 20*, 2007.
- M. Plummer, N. Best, K. Cowles, and K. Vines. CODA: Convergence diagnosis and output analysis for MCMC. *R News*, 6(1):7–11, March 2006.
- V. Rao and Y. W. Teh. Fast MCMC sampling for Markov jump processes and continuous time Bayesian networks. In *Proceedings of the Twenty-seventh Conference on Uncertainty in Artificial Intelligence (UAI)*, 2011a.
- V. Rao and Y. W. Teh. Gaussian process modulated renewal processes. In *Advances in Neural Information Processing Systems 23*, 2011b.
- V. Rao and Y. W. Teh. MCMC for continuous-time discrete-state systems. In *Advances in Neural Information Processing Systems, 24*, 2012.
- S. L. Scott and P. Smyth. The Markov modulated Poisson process and Markov Poisson cascade with applications to web traffic modeling. *Bayesian Statistics*, 7:1–10, 2003.
- C. Shelton, Y. Fan, W. Lam, J. Lee, and J. Xu. Continuous time Bayesian network reasoning and learning engine, 2010. <http://mloss.org/software/view/216/> .
- H. C. Tijms. *Stochastic Modelling and Analysis: a Computational Approach*. Wiley series in probability and mathematical statistics: Applied probability and statistics. Wiley, 1986. ISBN 9780471909118.
- D. J. Wilkinson. Stochastic modelling for quantitative description of heterogeneous biological systems. *Nature Reviews Genetics*, 10:122–133, 2009.